THE JOURNAL OF PHYSICAL CHEMISTRY C

Article

pubs.acs.org/JPCC

Multicomponent Assembly of Supramolecular Coordination Polygons on a Au(111) Surface

Tao Lin,[‡] Xue Song Shang,[†] Pei Nian Liu,*[,†] and Nian Lin*[,‡]

[†]Shanghai Key Laboratory of Functional Materials Chemistry and Institute of Fine Chemicals, East China University of Science and Technology, Meilong Road 130, Shanghai, China

[‡]Department of Physics, The Hong Kong University of Science and Technology, Clear Water Bay, Hong Kong, China

Supporting Information

ABSTRACT: We have studied the self-assembly of a series of multicomponent cyclic supramolecular polygons on a Au(111) surface using scanning tunneling microscopy and kinetic Monte Carlo simulations. Our results indicate that while closed polygons or cages efficiently self-assemble in three dimensions at appropriate temperatures and concentrations, chain structures are formed predominantly and the yield of cyclic polygon structures is very low in two dimensions independent of temperature and concentration. This substantial shift in the ring−chain equilibrium can be attributed to subtle competition between kinetic and thermodynamic controls. Simulations suggest that on a surface, where the translational and rotational freedom of the molecules are restricted and intramolecular bond flipping is hindered, the low-energy reaction pathways that are essential for the formation of cyclic structures are blocked. In addition, microscopy images suggest that surface defects provide kinetic traps that further reduce the yield of cyclic structures. Our findings reveal the striking differences between the on-surface self-assembly and solution self-assembly of discrete supramolecular systems.

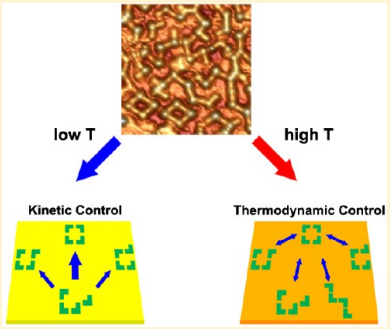

INTRODUCTION

Self-assembly of cyclic structures is of high interest in fundamental research and applications. Ring−chain competition in polymerization arises when equilibrium exists between the linear and cyclic forms of oligomers and polymers.[1−7] Cyclic assemblies predominate below the so-called critical polymerization concentration (CPC), while the concentration of cyclic species remains constant above the CPC, with the excess monomers producing mainly linear species.[1,2,7,8] Such competition deserves attention because it plays important roles in numerous synthetic processes, such as polymerization reactions[9−12] and polymer assembly via noncovalent interactions.[1,2,13−15] For example, if the competition is not properly controlled, normally by thermodynamics and/or kinetics controls, the desired products (cyclic or linear) will not be obtained in high yield.

Ring−chain competition is also important for supramolecular coordination self-assembly when the molecules can be assembled into discrete polygons or cages using metal−ligand coordination.[16−20] During the assembly processes, metastable intermediate products frequently form at the local minima on the reaction free energy hypersurface (FEHS). Depending on the morphology of the FEHS, self-assembly may be under kinetic or thermodynamic control under the particular assembly conditions.[17] When assembly is under thermodynamic control, intermediates can often be converted into stable low-energy target products if the reaction is allowed to proceed for a relatively long time or if annealing is performed at elevated temperatures.[21−23] If, however, the assembly is under kinetic control, a metastable product can remain kinetically trapped in a deep local minimum.[24−31]

Recent work has examined supramolecular self-assembly in two dimensions (2D), i.e., assembly confined to solid−liquid or solid−vacuum interfaces.[32−35] On one hand, 2D supramolecular self-assembly shows many of the same characteristics as the corresponding 3D processes. On the other hand, different behavior is expected as the molecules adsorbed on a surface must overcome translational or rotational energy barriers to find their destiny due to surface−molecule interactions;[35−40] thus, the molecules have fewer degrees of freedom in the 2D assembly processes than in the corresponding 3D ones. For example, the translational or rotational motions of intermediate supramolecules on a surface are greatly reduced and are even frozen at room temperature. In addition, torsional motion around a bond is prohibited for most species adsorbed on surfaces; in other words, molecules or molecular groups cannot flip on a surface. These limitations are expected to introduce deep local minima on the FEHS of 2D confined self-assembly, leading to the creation of thermodynamic minima or kinetic traps.

In the present work, we investigated the 2D self-assembly of multicomponent supramolecular cyclic structures on a Au(111) surface.[41−43] We chose ditopic pyridylporphyrin (**A** and **B**) and bis(terpyridine) (**C** and **D**) as ligands, which are linked by

Received: August 25, 2013
Revised: October 2, 2013
Published: October 2, 2013

   dx.doi.org/10.1021/jp408504b | J. Phys. Chem. C 2013, 117, 23027−23033

terpyridyl-Fe-pyridyl coordination (Chart 1).[44] **A** and **C** form three types of cyclic structures: six-component A_3C_3, eight-component A_4C_4, and 12-component A_6C_6. **A** and **D** form two types of cyclic structures: four-component A_2D_2 and six-component A_3D_3. **B** and **D** form the 12-component cyclic structure B_6D_6. In all cases, chain structures are formed together with the cyclic ones. We explored the ring−chain equilibrium by analyzing the effects of temperature, reactant concentrations, and component ratios on the yield of cyclic structures. We also modeled the 2D supramolecular assembly using kinetic Monte Carlo (KMC) simulation. Our results show that self-assembly of cyclic structures differs in several aspects in 2D and 3D; in particular, there exists deeper kinetic traps for the 2D case. We argue that subtle competition between kinetics and thermodynamics in 2D means that reaction conditions must be controlled more carefully, and some types of self-assembly may not proceed at all.

Chart 1. The Molecules Used in This Study (Ligands A−D) and the Corresponding Representations of Their Cyclic Structures

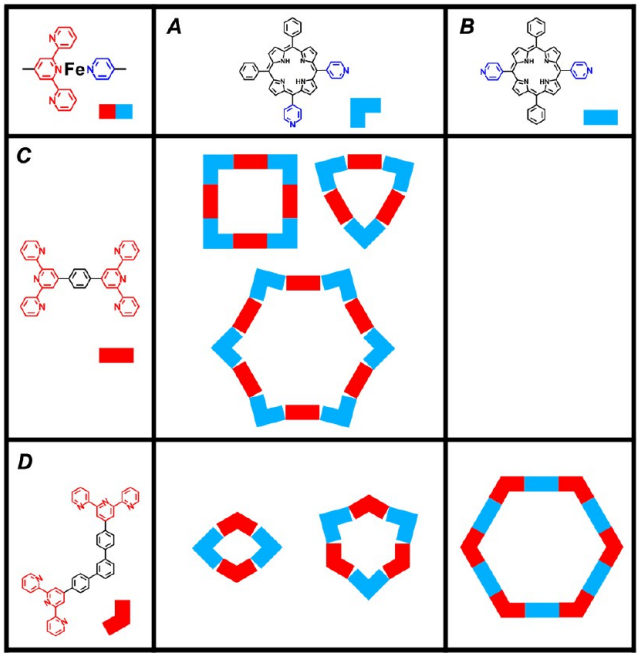

METHOD

Experiments were performed in an ultrahigh-vacuum system (Omicron Nanotechnology) with a base pressure below 5×10^{-10} mbar. A single-crystalline Au(111) substrate was cleaned by argon-ion sputtering and annealing to approximately 900 K. The molecules used in this study shown in Chart 1 were thermally evaporated by a molecular beam evaporator and deposited onto the Au(111) substrate, which was maintained at room temperature. The evaporation temperatures for these four molecules **A**, **B**, **C**, and **D** are 610, 590, 550, and 590 K, respectively. Scanning tunneling microscopy (STM) measurements were performed at 296 K.

Kinetic Monte Carlo (KMC) simulations were performed on a 100 × 100 square or hexagonal lattice using an algorithm previously described[45] with a periodic boundary condition imposed. Initially equal amounts of two kinds of molecules were deposited randomly onto the lattice. Desorption of the molecules was not allowed. Single molecules were allowed to hop to a nearest-neighbor site or rotate clockwise or anticlockwise by 90° on the square lattice or 60° on the hexagonal one. The rates of these events were determined by the corresponding energy barriers and temperature. A coordination bond was formed when a ligand encountered a complementary ligand in a head-to-head configuration. The bonds can be dissociated at a rate given by the bond strength and temperature.

RESULTS AND DISCUSSION

Experimental Results. Figure 1 shows representative high-resolution STM images of the six cyclic structures of A_2D_2, A_3D_3, B_6D_6, A_3C_3, A_4C_4, and A_6C_6 as well as the corresponding structural models. In these structures, the porphyrin ligands act as corners and the dogbone-shaped bis(terpyridine) ligands act as linkers. Some of the porphyrin molecules appear bright due to metalation of their macrocyclic core.[44−46] The formation of the cyclic structures occurred exclusively after mixing Fe with the two types of ligands, indicating that the structures are stabilized by terpyridyl-Fe-pyridyl coordination.[44] Fe atoms were not resolved in the STM topographs, presumably due to electronic effects.[47] A_3C_3, A_4C_4, and A_6C_6 contain the same ligand combinations, but with different coordination angles between two side linker ligands. For example, the A_4C_4 structure exhibits a rhombus shape with corner angles of 65°

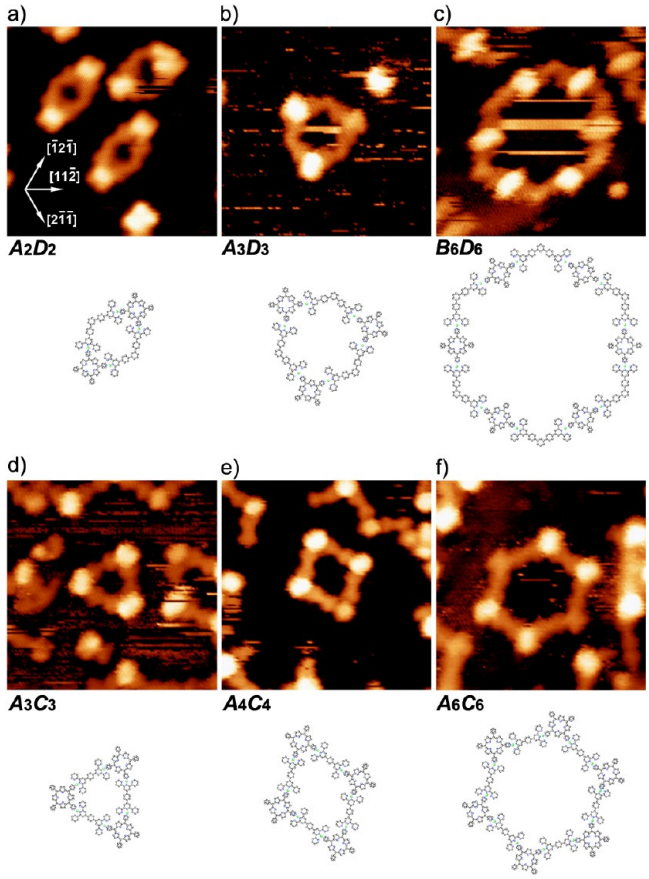

Figure 1. STM topographs of cyclic structures and the corresponding structural models of (a) A_2D_2, (b) A_3D_3, (c) B_6D_6, (d) A_3C_3, (e) A_4C_4, and (f) A_6C_6. All STM topographs are 15 × 15 nm^2.

dx.doi.org/10.1021/jp408504b | J. Phys. Chem. C 2013, 117, 23027−23033

and 115°, instead of a square shape with a corner angle of 90°. Similar results were obtained with A_2D_2 and A_3D_3. This nonideal geometry can be attributed to conformational flexibility of the on-surface coordination bond[42,48] and symmetry mismatch between the atomic lattice of the Au(111) substrate (6-fold) and the ideal cyclic structures.[42] Note that in the **A** + **D** system A_2D_2 and A_3D_3 are in comparable amounts, whereas in the **A** + **C** system, A_4C_4 is the main products while A_3C_3 and A_6C_6 are byproducts of less quantities. In the later sections, we will not analyze these two structures.

Figure 2a–c presents large views of STM images showing the structures assembled from three ligand combinations (**A** + **C**, **A** + **D**, and **B** + **D**) in the presence of Fe. In all three cases, zigzag chains are abundant, whereas cyclic structures (circled in the figure) are rare. We counted the numbers of different (cyclic and chain) structures over a total area of 10000 nm^2. The quantitative analysis of the structures showed that yield of the cyclic structures, defined as the percentage of the total amount of porphyrin ligands forming cyclic structures, is only 3.3% for A_2D_2, 2% for A_3D_3 and A_4C_4, and 0.8% for B_6D_6. The yield declined with increasing number of constituents in the cyclic structure (4, 6, 8, or 12). This trend implies that the probability of a ligand adopting a correct configuration required for assembling a large cyclic structure (e.g., appropriate molecular orientation) is lower than that for a smaller structure. We varied the ratio of the two ligands to optimize the self-assembly of the cyclic structures. Figure 3 shows the structures formed by **A** and **C** when mixed in **A**:**C** ratios of 2:1 and 1:2. The assembled structures are primarily small clusters and short oligomers. Only the stoichiometric 1:1 ratio resulted in the formation of extended polymeric structures (cf. Figure 2b). This observation manifests the importance of stoichiometry in the multicomponent self-assembly. We use the samples of stoichiometric 1:1 ratio when analyzing the products of ligand mixtures in the rest of this paper.

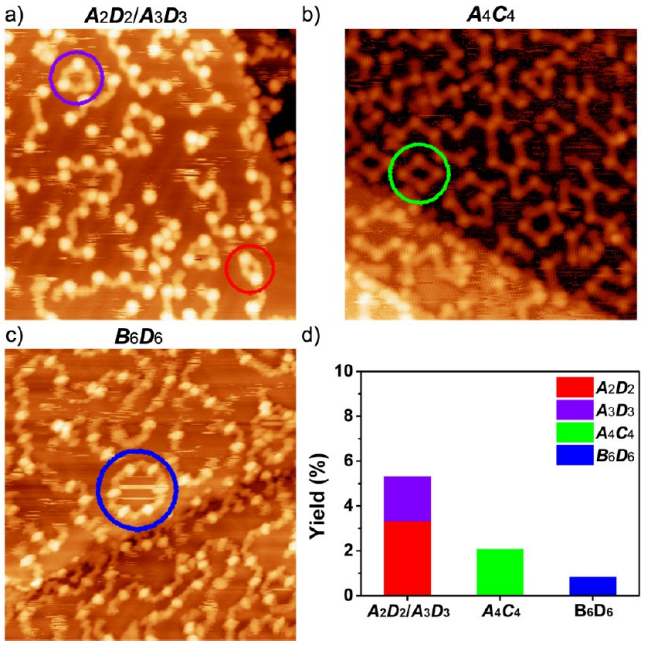

Figure 2. Large-view STM images of the self-assembled structures. (a–c) STM topographs (50 × 50 nm^2) showing abundant zigzag chains and low-yield cyclic structures in (a) **A** + **D**, (b) **A** + **C**, and (c) **B** + **D**. Representative cyclic structures are circled. (d) The yields of the different cyclic structures.

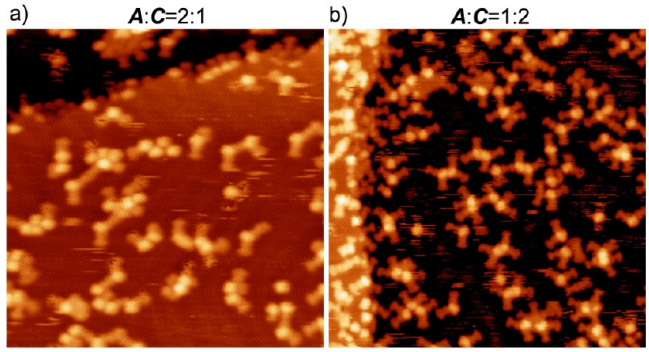

Figure 3. STM topographs (50 × 50 nm^2) showing the self-assembled structures of **A** + **C** mixed in different ratios: (a) **A**:**C** = 2:1 and (b) **A**:**C** = 1:2.

To explore how kinetics controls the self-assembly processes, we annealed **A** + **D** samples at different temperatures for different durations. Annealing at 400 K for 5 min gave low yields of the cyclic structures similar to those obtained without annealing. Extending the 400 K annealing to 2 h increased the yield of A_2D_2 more than 2-fold to 7.7% and the yield of A_3D_3 to 2.3% (Figure S1). Further annealing with longer time, however, did not enhance the yield, suggesting that the low yield can be ascribed to deep kinetic trapping. In order to overcome the kinetic limitation, we increased the annealing temperature to 450 K. Contrary to our expectations, only zigzag chains were observed (Figure S1). We suggest that the low yield may be ascribed to excessive ligand concentration, since cyclic structures are formed in high yield in 3D only when the ligand concentration is below the CPC. Therefore, we investigated **A** + **D** self-assembly over a broad range of concentrations. None of the ratios led to a significant increase in cyclic yield (data not shown). These findings suggest that while self-assembly of polygons can be highly efficient in 3D, their self-assembly is extremely inefficient in 2D. The formation of chain structures is strongly favored over that of ring structures in 2D. Apparently, this behavior may be attributed to the nonideal coordination geometry since the formation of cyclic structures might be thermodynamically less favored than the chain structures which contain ideal coordination ones. However, the B_6D_6 structures only contain ideal coordination geometry, but this structure behaves similarly as the rest. On the other hand, our previous study clearly demonstrated that in the assembly of extended 2D structures nonideal geometry also occurs; nevertheless, this effect does not hinder the self-assembly of the 2D structures with high yield. Thus, there must be other reasons accounting for the shifting of the ring–chain balance.

KMC Simulation. We carried out KMC simulations to gain insight into the mechanism of 2D self-assembly of the cyclic structures. We simulated four systems: 4-component A_2D_2, 6-component A_3D_3, 8-component A_4C_4, and 12-component B_6D_6. The substrate lattice was 6-fold for A_2D_2 (Figure 4a), A_3D_3 (Figure 4b), and B_6D_6 (Figure 4d) but 4-fold for A_4C_4 (Figure 4c). The translational (rotational) freedom of the molecules was constrained by a diffusion (rotational) barrier of E_d = 0.68 eV (E_r = 1.00 eV).[40,45] When two complementary ligands (yellow and light blue ends) encountered each other in a head-to-head configuration, a bond formed with a binding

dx.doi.org/10.1021/jp408504b | J. Phys. Chem. C 2013, 117, 23027–23033

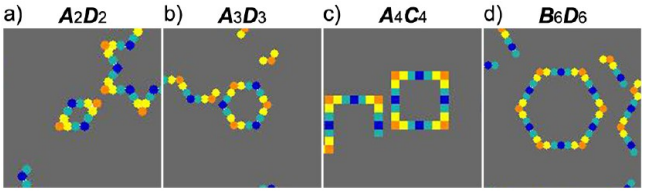

Figure 4. The four cyclic structures simulated using KMC. Each molecule consists of two ends (yellow or light blue) linked by a backbone (orange or dark blue). The backbone defines the molecular geometry. A yellow end could bond with a light blue end only if they encountered each other in head-to-head configuration.

energy of E_b = 0.30 eV. Flipping of the molecules (mirror operation) was not allowed.

Figure 5a–d displays representative simulation results obtained under conditions comparable to the experimental

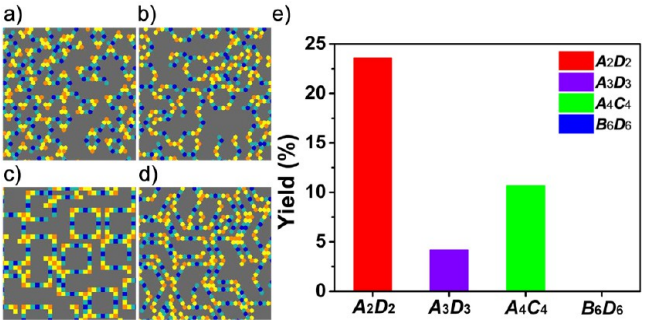

Figure 5. KMC-simulated self-assembly of (a) A_2D_2 (30% concentration), (b) A_3D_3 (30%), (c) A_4C_4 (36%), and (d) B_6D_6 (36%). All assemblies were subjected to annealing at 400 K for 5 min. (e) Yields of the respective cyclic structures.

ones including annealing temperature and duration, molecular concentration (percentage of substrate surface area covered by the molecules), and ligand ratio. Similar to the experiments, the simulations produced mixtures of cyclic structures and zigzag chain structures. The yields of the cyclic structures from the simulations were 23.6% for A_2D_2, 4.2% for A_3D_3, 10.6% for A_4C_4, and 0% for B_6D_6 (Figure 4d). Except for B_6D_6, the simulated yields of A_2D_2, A_3D_3, and A_4C_4 are higher than the experimental ones. Several factors may explain this discrepancy. First, when the samples were annealed at high temperature or with prolonged annealing duration, the Fe atoms that normally acted as coordination centers to link two complementary ligands may have nucleated into Fe islands or diffused into the Au crystal. The simulations did not take these effects into account. Second, the coordination angles in the experimental products often deviate from ideal geometry, which may reduce the binding strength. Third, A_4C_4 formed on a 6-fold substrate in the experiments, while it formed on a 4-fold substrate in the simulations. A 4-fold substrate matches the symmetry of the A_4C_4 structure and is therefore expected to lead to higher yield. Fourth, molecules in the experiments may have become trapped at surface defects such as step edges, Au(111) herringbone reconstruction, or Fe islands; in contrast, the molecules in the simulations moved freely on the substrate. Despite these differences, the simulations reproduced the key characteristics of the experimental results: most products are zigzag chain structures while cyclic structures form in very low yield. In this way, both experiments and simulation indicate that self-assembly of cyclic structures is much less favorable in 2D than in 3D, so we conclude that the ring–chain equilibrium is shifted toward chain formation. As in our experiments, we performed simulations to examine the effects of stoichiometry on self-assembly. We simulated self-assembly processes with **A** and **C** present in ratios of 2:1, 1:1, and 1:2 (always at the same total molecular concentration), and we compared the yields of the cyclic structure A_4C_4 obtained. The yield for the two nonstoichiometric ratios was approximately one-third of that for the stoichiometric 1:1 ratio (Figure S2). These results are consistent with the experimental observations (Figure 3).

Discussion. Self-assembly in 3D occurs through the stepwise formation of various intermediates that lead progressively to the final target structures. The (almost) unrestricted translational, rotational, and torsional freedom of individual molecules or intermediates in 3D provides many low-energy pathways on the FEHS. As a result, intermediates can easily find a low-energy pathway to convert into the target structures at ambient or slightly elevated temperatures. However, in 2D self-assembly, many of these low-energy pathways are blocked since translational, rotational, and torsional molecular motion is severely restricted. We propose that this restriction makes the 2D self-assembly of cyclic structures extremely inefficient. We illustrate this proposal in Scheme 1a: **I** is an intermediate en route to the target cyclic **IV**;

Scheme 1. (a) Kinetically Controlled Self-Assembly at Low Temperature, in Which II and III Are Kinetically Trapped Intermediates; (b) Thermodynamically Controlled Self-Assembly at High Temperature, in Which Configurational Entropy Prefers Chain Structures

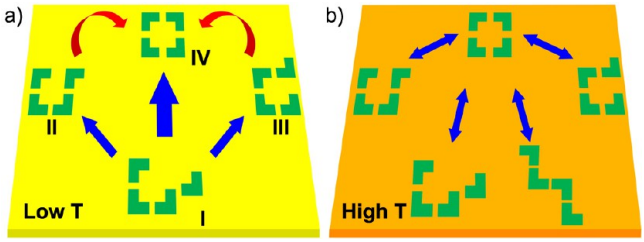

I can develop not only into **IV** but also into intermediates **II** or **III**. In 3D, **II** or **III** can easily reach the target structure by flipping around a bond and forming an intramolecular bond, a process indicated by the red curved arrows in Scheme 1a. On a 2D surface, however, flipping around a bond is greatly hindered, so **II** or **III** must convert back into **I** in order to reach the target structure **IV**. Since converting **II** or **III** into **I** involves energetically costly bond breaking, **II** and **III** lie in a deep kinetic trap on the FEHS. Thus, we propose that the FEHS of 2D self-assembly is highly corrugated as compared with the 3D one.

To test this proposal, we monitored time-lapse images of KMC-simulated self-assembly of cyclic structures. Figure 6 shows time-lapse images over 66 s of the assembly process of A_4C_4. An intermediate similar to **II** forms initially (red ellipse in Figure 6a). Subsequently, this intermediate develops into a chain structure (Figure 6b–f) instead of a cyclic structure. One may expect that if intramolecular bond flipping is allowed, the ligand at the upper-right corner in the circled structure in Figure 6a would bound with the ligand at the right side, forming a closed cyclic structure. To examine the effects of intramolecular bond flipping, we introduced flipping events into

dx.doi.org/10.1021/jp408504b | J. Phys. Chem. C 2013, 117, 23027–23033

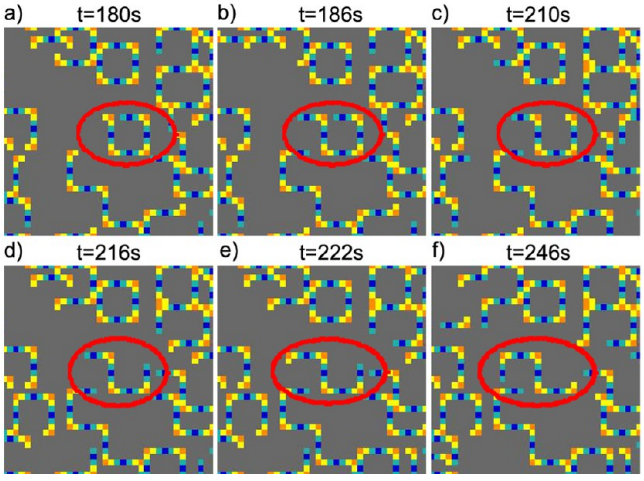

Figure 6. Simulated time-lapse images of KMC-simulated 2D self-assembly of $\mathbf{A}_4\mathbf{C}_4$ with annealing at 375 K. Red ellipses track the evolution of a typical intermediate structure.

the simulation by reducing the energy barrier of bond flipping. Again we chose the $\mathbf{A}_4\mathbf{C}_4$ system as the representative model system. Figure 7a displays the simulated yield of the cyclic

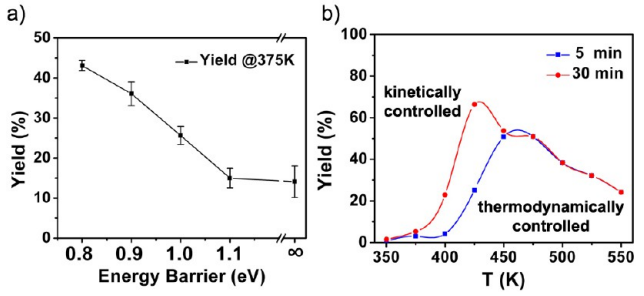

Figure 7. (a) KMC-simulated yield of cyclic structures of $\mathbf{A}_4\mathbf{C}_4$ (30% concentration, annealing at 375 K for 30 min) as a function of intramolecular bond flipping barrier. (b) KMC-simulated yields of the 2D self-assembly of cyclic $\mathbf{A}_3\mathbf{D}_3$ (24% concentration) as a function of annealing temperatures for 5 min (blue) and 30 min (red).

structure as a function of the energy barrier. One can find the yield of the cyclic structure increases when reducing the barrier, and when the barrier is 0.8 eV, the yield is almost tripled as compared to the situation without flipping. (Note in the simulations only L-shaped monomer can flip, and the flipping of dimer or even larger units was not considered due to technical difficulty.) Because of computational resource limitation, we did not perform the simulation of even low-energy barrier. Despite this limitation, the trend revealed in Figure 7a clearly indicates that the yield of the cyclic structures is substantially high in 3D self-assembly considering that the torsional rotation barrier of a C−C bond in free space is about 0.1 eV.[49] Hence, we conclude that hindered bond flipping in 2D significantly slows down the self-assembly of the cyclic structure. We also argue that bond flipping plays a very important role in the formation of cyclic structures in 3D self-assembly.

Performing annealing at higher temperatures is a common strategy to overcome kinetic controls. At higher temperature, trapped intermediates can gain sufficient energy to escape the kinetic traps and explore the FEHS in search of the thermodynamic minimum. Therefore, annealing may convert intermediates like **II** and **III** in Scheme 1a into the thermodynamically stable product **IV**. To test whether raising temperature can enhance the yield of the cyclic structures, we simulated the self-assembly of $\mathbf{A}_3\mathbf{D}_3$ with annealing in a temperatures range from 350 to 550 K for 5 min (blue curve) and 30 min (red curve) (Figure 7b). When the annealing temperature is below 400 K, time-lapse images of the simulation (data not shown) reveal that the molecules do not have sufficient energy to move effectively on the surface, and once chain structures form, they do not dissolve. Extending the time from 5 to 30 min can enhance the yield, confirming that the low yield can be attributed to kinetic controls. The simulated yield can be raised as high as 60% after 30 min annealing at 425 K. In the experiments, however, prolonged annealing only raised the yield to 10%. The neglecting of various experimental details in the simulations as discussed before presumably accounts for this discrepancy. Above 425 K, the yield declines with increasing temperature. At this stage, the self-assembly has reached thermodynamic equilibrium while the formed cyclic structures are frequently dissociated, as can be seen in the time-lapse simulation images. The Jacobson−Stockmayer theory predicts that the equilibrium between cyclic and chain polymers is determined solely by the change in configurational entropy associated with cyclization.[50] Thus, at sufficiently higher temperatures, the ring−chain equilibrium is expected to shift toward the chain structures, as illustrated in Scheme 1b, because entropy contribution becomes important at higher temperature. We attribute the decline of the yield at the high temperature regime to thermodynamic control.

The CPC appears to be a critical factor in the ring−chain competition during cyclic product formation. Therefore, we performed KMC simulations of the 2D self-assembly of $\mathbf{A}_3\mathbf{D}_3$ at different molecular concentrations (modeled in the simulation as surface area coverage). The simulated annealing was carried out at 450 K for 30 min to ensure that the reaction would be in thermodynamic equilibrium. At the extreme of very low concentrations, the molecules rarely encountered one another and therefore rarely formed cyclic structures (Figure 8a). At the

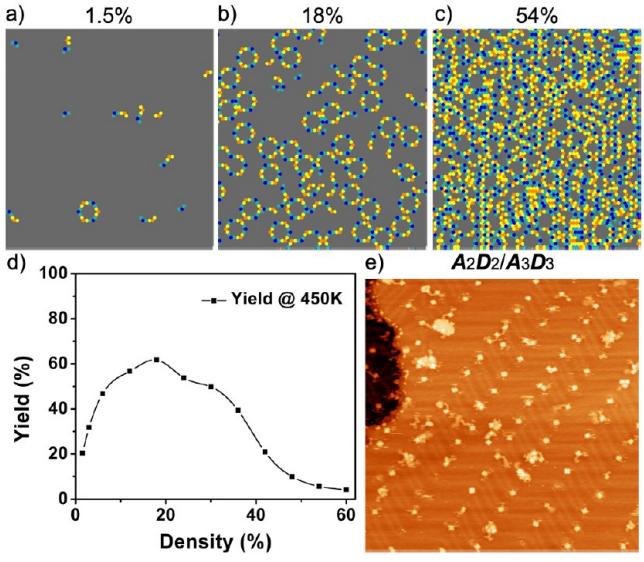

Figure 8. KMC-simulated self-assembly of **A** and **D** ligands at different concentrations: (a) 1.5%, (b) 18%, (c) 54%. (d) Yields of $\mathbf{A}_3\mathbf{D}_3$ as a function of concentration. (e) STM image (100 × 100 nm^2) showing the assembly of **A** and **D** present at concentration below the CPC.

dx.doi.org/10.1021/jp408504b | J. Phys. Chem. C 2013, 117, 23027−23033

extreme of very high concentrations, the molecules could not move freely on the substrate for lack of available space, again preventing them from forming cyclic species (Figure 8c). At intermediate concentrations, these effects were less severe, and the yield of cyclic product was relatively high (Figure 8b). Analysis of the yield of the cyclic structures as a function of concentration (Figure 8d) shows that the yield rises quickly at low concentrations, reaching a maximum of 60% yield at 18% coverage, and then declining at high concentrations. These results are consistent with the studies of the effects of CPC on ring−chain competition. Experimentally, we did not observe a significant yield enhancement over a wide range of ligand concentrations including below the CPC. The STM data provide us some clues why this happens: Figure 8e is a representative STM image of the self-assembly in which the molecule concentration is below the CPC. One can see that the molecules are trapped at the elbow sites of the Au(111) herringbone reconstruction or step edges. Thus, we argue that the surface defects, which effectively trap molecules, hinder the high-yield formation of the cyclic structures below the CPC.

CONCLUSIONS

We have investigated the self-assembly of a series of cyclic structures on a Au(111) surface using STM and KMC simulation. The yield of closed polygon structures in 2D is much lower than in 3D. KMC simulations suggest that this low yield can be attributed to a subtle competition between kinetic and thermodynamic control: chain structures predominate at low temperature due to deep kinetic traps arising from of the restricted molecular motion in 2D, whereas at high temperature, thermodynamics (entropy) favors chain structures. This dilemma inherently constrains the formation of the cyclic structures and consequently shifts the ring−chain equilibrium. We propose that to drive the systems to a thermodynamic equilibrium state, one must reduce surface−molecule interaction, i.e., open the low-energy reaction pathways on the FEHS.

ASSOCIATED CONTENT

Supporting Information

Synthesis sample of **A** + **D** under series annealing treatments and simulation of **A** + **C** with different **A**:**C** ratios. This material is available free of charge via the Internet at http://pubs.acs.org.

AUTHOR INFORMATION

Corresponding Authors

*Tel 852-23587494; e-mail phnlin@ust.hk (N.L.).
*Tel 021-64250552; e-mail liupn@ecust.edu.cn (P.N.L.).

Notes

The authors declare no competing financial interest.

ACKNOWLEDGMENTS

This work was supported financially by the Hong Kong Research Grants Council (project no. 602712), the National Natural Science Foundation of China (project nos. 21172069 and 21190033), the Innovation Program of Shanghai Municipal Education Commission (project no. 12ZZ050), and the Fundamental Research Funds for the Central Universities.

REFERENCES

(1) Ten Cate, A. T.; Kooijman, H.; Spek, A. L.; Sijbesma, R. P.; Meijer, E. W. Conformational Control in the Cyclization of Hydrogen-Bonded Supramolecular Polymers. *J. Am. Chem. Soc.* **2004**, *126*, 3801−3808.
(2) De Greef, T. F. A.; Ercolani, G.; Ligthart, G. B. W. L.; Meijer, E. W.; Sijbesma, R. P. Influence of Selectivity on the Supramolecular Polymerization of AB-Type Polymers Capable of Both A·A and A·B Interactions. *J. Am. Chem. Soc.* **2008**, *130*, 13755−13764.
(3) Xu, J.; Fogleman, E. A.; Craig, S. L. Structure and Properties of DNA-Based Reversible Polymers. *Macromolecules* **2004**, *37*, 1863−1870.
(4) Ohga, K.; Takashima, Y.; Takahashi, H.; Kawaguchi, Y.; Yamaguchi, H.; Harada, A. Preparation of Supramolecular Polymers from a Cyclodextrin Dimer and Ditopic Guest Molecules: Control of Structure by Linker Flexibility. *Macromolecules* **2005**, *38*, 5897−5904.
(5) Bastings, M. M. C.; de Greef, T. F. A.; van Dongen, J. L. J.; Merkx, M.; Meijer, E. W. Macrocyclization of Enzyme-Based Supramolecular Polymers. *Chem. Sci.* **2010**, *1*, 79−88.
(6) Xiao, T.; Feng, X.; Ye, S.; Guan, Y.; Li, S.-L.; Wang, Q.; Ji, Y.; Zhu, D.; Hu, X.; Lin, C.; Pan, Y.; Wang, L. Highly Controllable Ring−Chain Equilibrium in Quadruply Hydrogen Bonded Supramolecular Polymers. *Macromolecules* **2012**, *45*, 9585−9594.
(7) Ercolani, G.; Mandolini, L.; Mencarelli, P.; Roelens, S. Macrocyclization under Thermodynamic Control. A Theoretical Study and Its Application to the Equilibrium Cyclooligomerization of β-Propiolactone. *J. Am. Chem. Soc.* **1993**, *115*, 3901−3908.
(8) Ercolani, G. Physical Basis of Self-Assembly Macrocyclizations. *J. Phys. Chem. B* **1998**, *102*, 5699−5703.
(9) Gordon, M.; Temple, W. B. Ring-Chain Competition Kinetics in Linear Polymers. *Makromol. Chem.* **1972**, *152*, 277−289.
(10) Kricheldorf, H. R.; Böhme, S.; Schwarz, G. Macrocycles. 17. The Role of Cyclization in Kinetically Controlled Polycondensations. 2. Polyamides. *Macromolecules* **2001**, *34*, 8879−8885.
(11) Kricheldorf, H. R.; Böhme, S.; Schwarz, G.; Krüger, R.-P.; Schulz, G. Macrocycles. 18. The Role of Cyclization in Syntheses of Poly(ether-sulfone)s. *Macromolecules* **2001**, *34*, 8886−8893.
(12) Jia, Z.; Monteiro, M. J. Cyclic Polymers: Methods and Strategies. *J. Polym. Sci., Part A: Polym. Chem.* **2012**, *50*, 2085−2098.
(13) Hofmeier, H.; Hoogenboom, R.; Wouters, M. E. L.; Schubert, U. S. High Molecular Weight Supramolecular Polymers Containing Both Terpyridine Metal Complexes and Ureidopyrimidinone Quadruple Hydrogen-Bonding Units in the Main Chain. *J. Am. Chem. Soc.* **2005**, *127*, 2913−2921.
(14) Wilson, A. J. Non-covalent Polymer Assembly Using Arrays of Hydrogen-Bonds. *Soft Matter* **2007**, *3*, 409−425.
(15) Chen, C.-C.; Dormidontova, E. E. Ring-Chain Equilibrium in Reversibly Associated Polymer Solutions: Monte Carlo Simulations. *Macromolecules* **2004**, *37*, 3905−3917.
(16) Chakrabarty, R.; Mukherjee, P. S.; Stang, P. J. Supramolecular Coordination: Self-Assembly of Finite Two- and Three-Dimensional Ensembles. *Chem. Rev.* **2011**, *111*, 6810−6918.
(17) Cook, T. R.; Zheng, Y.-R.; Stang, P. J. Metal-Organic Frameworks and Self-Assembled Supramolecular Coordination Complexes: Comparing and Contrasting the Design, Synthesis and Functionality of Metal-Organic Materials. *Chem. Rev.* **2013**, *113*, 734−777.
(18) Fujita, M.; Yazaki, J.; Ogura, K. Preparation of a Macrocyclic Polynuclear Complex, $((en)Pd(4,4'\text{-bpy}))_4(NO_3)_8$, Which Recognizes an Organic Molecule in Aqueous Media. *J. Am. Chem. Soc.* **1990**, *112*, 5645−5647.
(19) Stang, P. J.; Cao, D. H. Transition Metal Based Cationic Molecular Boxes. Self-Assembly of Macrocyclic Platinum(II) and Palladium(II) Tetranuclear Complexes. *J. Am. Chem. Soc.* **1994**, *116*, 4981−4982.
(20) Sun, Q.-F.; Iwasa, J.; Ogawa, D.; Ishido, Y.; Sato, S.; Ozeki, T.; Sei, Y.; Yamaguchi, K.; Fujita, M. Self-Assembled $M_{24}L_{48}$ Polyhedra and Their Sharp Structural Switch upon Subtle Ligand Variation. *Science* **2010**, *328*, 1144−1147.
(21) Zheng, Y.-R.; Stang, P. J. Direct and Quantitative Characterization of Dynamic Ligand Exchange between Coordination-Driven

Self-Assembled Supramolecular Polygons. *J. Am. Chem. Soc.* **2009**, *131*, 3487−3489.
(22) Sato, S.; Ishido, Y.; Fujita, M. Remarkable Stabilization of $M_{12}L_{24}$ Spherical Frameworks through the Cooperation of 48 Pd(II)-Pyridine Interactions. *J. Am. Chem. Soc.* **2009**, *131*, 6064−6065.
(23) Seidel, S. R.; Stang, P. J. High-Symmetry Coordination Cages via Self-Assembly. *Acc. Chem. Res.* **2002**, *35*, 972−983.
(24) Rivetti, C.; Guthold, M.; Bustamante, C. Scanning Force Microscopy of DNA Deposited onto Mica: Equilibration versus Kinetic Trapping Studied by Statistical Polymer Chain Analysis. *J. Mol. Biol.* **1996**, *264*, 919−932.
(25) Cui, H.; Chen, Z.; Zhong, S.; Wooley, K. L.; Pochan, D. J. Block Copolymer Assembly via Kinetic Control. *Science* **2007**, *317*, 647−650.
(26) Gosal, W. S.; Morten, I. J.; Hewitt, E. W.; Smith, D. A.; Thomson, N. H.; Radford, S. E. Competing Pathways Determine Fibril Morphology in the Self-assembly of β_2-Microglobulin into Amyloid. *J. Mol. Biol.* **2005**, *351*, 850−864.
(27) Hagan, M. F.; Elrad, O. M.; Jack, R. L. Mechanisms of Kinetic Trapping in Self-Assembly and Phase Transformation. *J. Chem. Phys.* **2011**, *135*, 104115.
(28) Baletto, F.; Doye, J. P. K.; Ferrando, R. Evidence of Kinetic Trapping in Clusters of C_{60} Molecules. *Phys. Rev. Lett.* **2002**, *88*, 075503.
(29) Royall, C. P.; Williams, S. R.; Ohtsuka, T.; Tanaka, H. Direct Observation of a Local Structural Mechanism for Dynamic Arrest. *Nat. Mater.* **2008**, *7*, 556−561.
(30) Korevaar, P. A.; George, S. J.; Markvoort, A. J.; Smulders, M. M. J.; Hilbers, P. A. J.; Schenning, A. P. H. J.; de Greef, T. F. A.; Meijer, E. W. Pathway Complexity in Supramolecular Polymerization. *Nature* **2012**, *481*, 492−496.
(31) Boekhoven, J.; Poolman, J. M.; Maity, C.; Li, F.; van der Mee, L.; Minkenberg, C. B.; Mendes, E.; van Esch, J. H.; Eelkema, R. Catalytic Control over Supramolecular Gel Formation. *Nat. Chem.* **2013**, *5*, 433−437.
(32) De Feyter, S.; de Schryver, F. C. Self-Assembly at the Liquid/Solid Interface: STM Reveals. *J. Phys. Chem. B* **2005**, *109*, 4290−4302.
(33) Stepanow, S.; Lin, N.; Barth, J. V. Modular Assembly of Low-Dimensional Coordination Architectures on Metal Surfaces. *J. Phys.: Condens. Matter* **2008**, *20*, 184002.
(34) Lin, N.; Stepanow, S.; Ruben, M.; Barth, J. V. Surface-Confined Supramolecular Coordination Chemistry. *Top. Curr. Chem.* **2009**, *287*, 1−44.
(35) Barth, J. V. Molecular Architectonic on Metal Surfaces. *Annu. Rev. Phys. Chem.* **2007**, *58*, 375−407.
(36) Schunack, M.; Linderoth, T. R.; Rosei, F.; Lægsgaard, E.; Stensgaard, I.; Besenbacher, F. Long Jumps in the Surface Diffusion of Large Molecules. *Phys. Rev. Lett.* **2002**, *88*, 156102.
(37) Otero, R.; Hümmelink, F.; Sato, F.; Legoas, S. B.; Thostrup, P.; Lægsgaard, E.; Stensgaard, I.; Galvão, D. S.; Besenbacher, F. Lock-and-Key Effect in the Surface Diffusion of Large Organic Molecules Probed by STM. *Nat. Mater.* **2004**, *3*, 779−782.
(38) Lauhon, L. J.; Ho, W. Single Molecule Thermal Rotation and Diffusion: Acetylene on Cu(001). *J. Chem. Phys.* **1999**, *111*, 5633−5636.
(39) Buchner, F.; Xiao, J.; Zillner, E.; Chen, M.; Röckert, M.; Ditze, S.; Stark, M.; Steinrück, H.-P.; Gottfried, J. M.; Marbach, H. Diffusion, Rotation, and Surface Chemical Bond of Individual 2H-Tetraphenylporphyrin Molecules on Cu(111). *J. Phys. Chem. C* **2011**, *115*, 24172−24177.
(40) Li, Y.; Lin, N. Combined Scanning Tunneling Microscopy and Kinetic Monte Carlo Study on Kinetics of Cu-Coordinated Pyridyl-Porphyrin Supramolecular Self-Assembly on a Au(111) Surface. *Phys. Rev. B* **2011**, *84*, 125418.
(41) Yokoyama, T.; Yokoyama, S.; Kamikado, T.; Okuno, Y.; Mashiko, S. Selective Assembly on a Surface of Supramolecular Aggregates with Controlled Size and Shape. *Nature* **2001**, *413*, 619−621.
(42) Heim, D.; Seufert, K.; Auwärter, W.; Aurisicchio, C.; Fabbro, C.; Bonifazi, D.; Barth, J. V. Surface-Assisted Assembly of Discrete Porphyrin-Based Cyclic Supramolecules. *Nano Lett.* **2010**, *10*, 122−128.
(43) Wang, W.; Wang, S.; Hong, Y.; Tang, B. Z.; Lin, N. Selective Supramolecular Assembly of Multifunctional Ligands on a Cu(111) Surface: Metallacycles, Propeller Trimers and Linear Chains. *Chem. Commun.* **2011**, *47*, 10073−10075.
(44) Shi, Z.; Lin, N. Structural and Chemical Control in Assembly of Multicomponent Metal-Organic Coordination Networks on a Surface. *J. Am. Chem. Soc.* **2010**, *132*, 10756−10761.
(45) Gottfried, J. M.; Marbach, H. Surface-Confined Coordination Chemistry with Porphyrins and Phthalocyanines: Aspects of Formation, Electronic Structure, and Reactivity. *Z. Phys. Chem.* **2009**, *223*, 53−74.
(46) Li, Y.; Xiao, J.; Shubina, T. E.; Chen, M.; Shi, Z.; Schmid, M.; Steinrück, H.-P.; Gottfried, J. M.; Lin, N. Coordination and Metalation Bifunctionality of Cu with 5,10,15,20-Tetra(4-pyridyl)porphyrin Toward a Mixed-Valence Two-Dimensional Coordination Network. *J. Am. Chem. Soc.* **2012**, *134*, 6401−6408.
(47) Classen, T.; Fratesi, G.; Costantini, G.; Fabris, S.; Stadler, F. L.; Kim, C.; de Gironcoli, S.; Baroni, S.; Kern, K. Templated Growth of Metal−Organic Coordination Chains at Surfaces. *Angew. Chem., Int. Ed.* **2005**, *44*, 6142−6145.
(48) Heim, D.; Écija, D.; Seufert, K.; Auwärter, W.; Aurisicchio, C.; Fabbro, C.; Bonifazi, D.; Barth, J. V. Self-Assembly of Flexible One-Dimensional Coordination Polymers on Metal Surfaces. *J. Am. Chem. Soc.* **2010**, *132*, 6783−6790.
(49) Pauling, L. The Nature of Bond Orbitals and the Origin of Potential Barriers to Internal Rotation in Molecules. *Proc. Natl. Acad. Sci. U. S. A.* **1958**, *44*, 211−216.
(50) Jacobson, H.; Stockmayer, W. H. Intramolecular Reaction in Polycondensations. I. The Theory of Linear Systems. *J. Chem. Phys.* **1950**, *18*, 1600−1606.